CHAPTER 2
THEORETICAL FRAMEWORK

In the field of gas sensing mechanisms, a profound understanding of the intricate interactions between gas molecules and carbon nanoclusters is paramount. These interactions form the bedrock upon which efficient gas sensors are built. While experimental procedures can yield valuable insights, they often demand substantial investments of time and finances. Computational approaches emerge as a potent and cost-effective avenue to delve into these molecular interactions at the atomic level. In this chapter, we delve into the computational methodologies essential to our gas sensing research. One of our primary tools is Gaussian 09 [1], employed for Density Functional Theory (DFT) calculations, a cornerstone in the study of molecular interactions.

This strategic junction not only opens the system's static attributes but also gives us access to its dynamic behaviour. It enables us to investigate time-dependent perturbation reactions and dig into the world of rheological properties, a multidimensional realm that includes electrical subtleties, structural dynamics, vibrational patterns, and crucial transfer parameters. This chapter provides a critical link to a thorough understanding of the molecular complexities that regulate gas interactions at the atomic scale, bringing us closer to the construction of highly efficient gas sensors.

2.1. Theory of Electronic Structure

2.1.1. Quantum Mechanics, Schrödinger Equation

The wave function $\Psi(\{r_i\}, \{R_A\})$ is utilised to construct a many-body system with N interacting electrons and M interacting ions. Ψ depends on both the electronic coordinates $\{r_i\}$ and the nuclear coordinates $\{R_A\}$, and is the solution to the Schrödinger equation [2] that is time-independent. Its non-relativistic form can be expressed as

$$\hat{H}\psi = E\psi \text{ ---- (2.1)}$$

$\hat{H}$: Hamiltonian operator

E: total energy of the system

The Hamiltonian consists of five terms:

$$\hat{H} = \hat{T_e} + \hat{T_A} + \hat{V_{ae}} + \hat{V_{ee}} + \hat{V_{AA}} \text{ ---- (2.2)}$$

Where,

$\widehat{T_e} = -\sum_{i=1}^{N} \frac{\hbar^2 \nabla_i^2}{2M_e}$: kinetic energy of electrons

$\widehat{T_A} = -\sum_{A=1}^{M} \frac{\hbar^2 \nabla_A^2}{2M_A}$: kinetic energy of ions

$\widehat{V_{Ae}} = -\sum_{i=1}^{N} \sum_{A=1}^{M} \frac{e^2 Z_A}{|r_i - R_A|}$: attractive energy between electrons and ions

$\widehat{V_{ee}} = \sum_{i=1}^{N} \sum_{j>1}^{N} \frac{e^2}{|r_i - r_j|}$: repulsive energy between electrons

$\widehat{V_{AA}} = \sum_{A=1}^{M} \sum_{B>A}^{M} \frac{e^2 Z_A Z_B}{|R_A - R_B|}$: repulsive energy between ions

Now, the Schrodinger equation becomes,

$$\left[-\sum_{i=1}^{N} \frac{\hbar^2 \nabla_i^2}{2M_e} - \sum_{A=1}^{M} \frac{\hbar^2 \nabla_A^2}{2M_A} - \sum_{i=1}^{N} \sum_{A=1}^{M} \frac{e^2 Z_A}{|r_i - R_A|} + \sum_{i=1}^{N} \sum_{j>1}^{N} \frac{e^2}{|r_i - r_j|} + \sum_{A=1}^{M} \sum_{B>A}^{M} \frac{e^2 Z_A Z_B}{|R_A - R_B|}\right] \psi = E\psi \text{ ---- (2.3)}$$

2.1.2. Born-Oppenheimer Approximation

Since equation (2.3) is difficult to solve, it becomes necessary to introduce some kind of approximation to solve it. The first one is called "Born-Oppenheimer approximation" (BO approximation) [3]. It relies upon the fact that the nucleons are about 1800 times heavier than the electrons. However, the kinetic energy of nucleons would be much lesser as compared to that of the nucleons. Therefore, the BO approximation neglects the kinetic energy term of nucleons, and allows us to dissociate the kinetic energies of electrons and ions. This implies that the nuclei are frozen in such configuration, which reduces the difficulty of solving the electron dynamics. The wave function then becomes:

$$\psi(\{r_i\}, \{R_A\}) = \psi(\{r_i\}) \times \psi(\{R_A\}) \text{ ---- (2.4a)}$$

$$H_e \psi(\{r_i\}) = E_e \psi(\{r_i\}) \text{ ---- (2.4b)}$$

Where, $H = -\sum_{i=1}^{N} \frac{\hbar^2 \nabla_i^2}{2M_e} - \sum_{i=1}^{N} \sum_{A=1}^{M} \frac{e^2 Z_A}{|r_i - R_A|} + \sum_{i=1}^{N} \sum_{j>1}^{N} \frac{e^2}{|r_i - r_j|} + \sum_{A=1}^{M} \sum_{B>A}^{M} \frac{e^2 Z_A Z_B}{|R_A - R_B|}$.

However, there are more simplifications needed as equation set (2.4) is difficult to solve.

The **Slater Determinant** [4] is introduced to for the free electrons of the system which satisfies the Pauli's exclusion principle. The wave function ψ is not an observable anymore and

$|\psi|^2 dx$ represents the probability of finding an electron in a given point in space $d\boldsymbol{x_i}$ *(i=1,…,N)*. The electron exchange will only invert the sign as electrons are identical:

$$\psi(\boldsymbol{x_i}) = -\psi(\boldsymbol{x_i}) \text{ ---- (2.5)}$$

However, the probability remains the same:

$$|\psi(\boldsymbol{x_i})|^2 = |\psi(\boldsymbol{x_i})|^2 \text{ ---- (2.6)}$$

A set of wave functions for a collection of electrons can be written as $X_i(\boldsymbol{x_i})$. The Slater determinant for N-electron system is given by:

$$\phi_{SD} = \frac{1}{\sqrt{N!}} \begin{vmatrix} X_1(\boldsymbol{x_1}) & \cdots & X_N(\boldsymbol{x_1}) \\ \vdots & \ddots & \vdots \\ X_i(\boldsymbol{x_N}) & \cdots & X_N(\boldsymbol{x_N}) \end{vmatrix} \text{ ---- (2.7)}$$

2.1.3. Hartree-Fock Method

Whenever the N-body wave function and determination of energy of a system becomes complicated to solve, the "Hartree-Fock (HF) method" is introduced [5-6]. The Fock Hamiltonian is given by:

$$f_i = -\frac{1}{2}\nabla_i^2 - \sum_k^{core} \frac{Z_k}{r_{ik}} + V_i^{HF} \text{ ---- (2.8)}$$

V_i^{HF} is the HF potential and it represents the average repulsive potential of one electron to the other *N-1* electrons. It is given by:

$$V_i^{HF}(\boldsymbol{x_1}) = \sum_i^N (\widehat{J_i}(\boldsymbol{x_1}) - \widehat{K_i}(\boldsymbol{x_1})) \text{ ---- (2.9)}$$

Where, $\boldsymbol{x_1}$ is the position of single electron, $\widehat{J_i}$ is the Coulomb operator, and $\widehat{K_i}$ is the exchange contribution to the HF potential, it is defined when it is operating on spin orbital.

$\widehat{J_i}$ and $\widehat{K_i}$ are defined as:

$$\widehat{J_i}(\boldsymbol{x_1}) = \int \left| X_j\left(\boldsymbol{x_{\frac{i}{2}}}\right) \right|^2 \left(\frac{1}{r_{12}}\right) d\boldsymbol{x_2} \text{ ---- (2.10a)}$$

$$\widehat{K_j}(\boldsymbol{x_1}) X_i(\boldsymbol{x_1}) = \int \left(X_j^*(\boldsymbol{x_2})\right)^2 \left(\frac{1}{r_{12}}\right) \left(X_i(\boldsymbol{x_2})\right) d\boldsymbol{x_2} X_i(\boldsymbol{x_1}) \text{ ---- (2.10b)}$$

This makes the HF potential V_i^{HF} non-local and dependent on initial unknown spin orbitals. A Hartree-Fock Self-Consistent Field (HF-SCF) technique is utilised to determine the V_i^{HF}. A new V_i^{HF} is produced using an initial set of spin orbitals (X_i), which are mathematically

conjectured. Then, new spin orbitals are calculated using this HF potential. The cycle is continued until the outcome satisfies the convergence criteria. The HF energy is more than the total energy because the HF approach does not take into account the dynamic correlation between electronic movements.

2.1.4. Density Functional Theory

The total density of electrons is used as a fundamental parameter in Density Functional Theory (DFT), rather than the electrons' N-body wave functions. A physical property is the electron density. It is simpler to calculate as the number of electrons rises. More significantly, this approach gets beyond the Hartree-Fock method's main drawback of ignoring electron correlation. As a result, DFT considerably increases computation accuracy, whereas the exchange part in HF method is well defined.

The first fundamental theorem of DFT was proposed by Hohenberg and Kohn [7-8], and their key premise was that "the external potential V_{ext} applied on the system is an external potential to the system which is due to the presence of the nuclei is a unique functional of the electronic density $\rho(\boldsymbol{r})$."

"The functional $F_H[\rho]$ that provides the ground state energy of the system delivers the lowest energy if and only if the input density corresponds to the actual ground state density", as per Hohenberg and Kohn's second fundamental theorem of DFT.

2.1.5. Kohn-Sham Equations

In 1965, Walter Kohn and Lu Jeu Sham came up with a method to solve the Schrodinger equation [9]. Considering they hypothesised that the electronic ground states remained the same, they replaced the interactive system with a non-interactive one. The density p(r) can be used to explain all of the contributions to the total energy. The energy is at its lowest and corresponds to the ground state only when the density is at its fundamental level, $\rho(\boldsymbol{r}) = \rho_0(\boldsymbol{r})$. The electron clouds' overall energy can be expressed as:

$$E[\rho] = T[\rho] + V_{ee}[\rho] + E_{XC}[\rho] + \int V_{ext}(\boldsymbol{r})\rho(\boldsymbol{r})d^3\boldsymbol{r} \text{ ---- (2.11)}$$

Where,

$T[\rho]$: kinetic energy of electrons without interactions

$V_{ee}[\rho]$: classical Coulombic interaction term

$E_{XC}[\rho]$: exchange correlation term

$\int V_{ext}(r)\rho(r)d^3r$: interaction between the electrons and the nuclei's external potential

As currently understood, the Density Functional Theory is exact since it is devoid of approximations. E [ρ], the exchange-correlation term, is the only undetermined term. It must be approximated, and the next section describes various approximations.

2.2. Exchange-Correlation Functionals

The exchange and correlation term, E[ρ], is a crucial component in density functional theory (DFT) calculations. It represents the total energy of a system and includes the exchange and correlation effects. Two commonly used methods for approximating E[ρ] in DFT calculations are Generalized Gradient Approximation (GGA) and Local Density Approximation (LDA). GGAs provide a more accurate description of exchange-correlation effects, while LDA is computationally efficient but less accurate for systems with strong electron-electron correlations or bond energies.

2.2.1. Local Density Approximation (LDA)

The LDA approach [10] suggests that the charge density ranges gradually on an atomic scale and that inhomogeneous electronic systems can be viewed as locally homogeneous by treating the electrons as a uniform electron gas. The exchange-correlation energy for a spin-unpolarized system can be expressed as:

$$E_{XC}^{LDA}[\rho] = \int \rho(\boldsymbol{r})\varepsilon_{XC}(\rho)d\boldsymbol{r} \text{ ---- (2.12)}$$

As one of the instances of the LDA functional, Vosko, Wilk, and Nusair (VWN) produced a Monte Carlo computation for a uniform electron gas. The local spin density approximation (LSDA) for the spin-polarized system can be used to express the exchange-correlation energy as follows:

$$E_{XC}^{LSDA}[\rho, \rho_B] = \int \rho(\boldsymbol{r})\varepsilon_{XC}(\rho, \rho_B)d\boldsymbol{r} \text{ ---- (2.13)}$$

Where, ρ, ρ_B are electronic densities. For computing molecular attributes like structures, vibrational frequencies, charge and dipole moments, etc., equation (2.13) offers an acceptable degree of precision. However, it turns out to be a poor approximation for energetic properties, such as binding energies, energy barriers, etc., when the density varies quickly.

2.2.2. Generalized Gradient Approximation (GGA)

The Generalized Gradient Approximation (GGA) [11] has been suggested as a solution to the prior issue. By treating the system as a non-uniform electron gas and accounting for non-local electron effects in the functional, it enhances the LDA technique. As a function of ρ and **∇**ρ, the exchange-correlation term can be expressed as follows:

$$E_{XC}^{GGA}[\rho] = \int \varepsilon_{XC}(\boldsymbol{r})[\rho(\boldsymbol{r}) + \boldsymbol{\nabla}\rho(\boldsymbol{r})]d^3\boldsymbol{r} \text{ ---- (2.14)}$$

Different approximations for the aforementioned equation can be used to construct the GGA family members, which includes BLYP, PW91, PBE, and other functionals [11-13]. GGA typically produces better results than LDA in terms of total energies, atomization energies, energy barriers, and structural energy differences since it allows for a broader range of variation. A better gradient-corrected GGA functional is the PBE functional (the exchange-correlation functional developed by Perdew, Burke, and Ernzerhof). All of the parameters in its straightforward derivation are fundamental constants. This functional, which is used in the current work, is most frequently used to both liquid molecules and solids.

2.2.3. Meta-GGA

With additional dependency on the Kohn-Sham kinetic energy density, the meta-GGA functionals [14] slightly improve the GGA functionals:

$$\tau(\boldsymbol{r}) = \sum_i \frac{1}{2}|\boldsymbol{\nabla}\varphi_i(\boldsymbol{r})|^2 \text{ ---- (2.15a)}$$

$$E_{XC}^{meta-GGA}[\rho] = \int \varepsilon_{XC}(\boldsymbol{r})[\rho(\boldsymbol{r}) + \boldsymbol{\nabla}\rho(\boldsymbol{r})]d^3\boldsymbol{r} \text{ ---- (2.15b)}$$

One of the most popular meta-GGA functionals is the TPSS functional, which was created by Tao, Perdew, Staroverov, and Scuseria.

2.2.4. Hybrid Functionals

The exchange terms of the previously mentioned functionals are poorly defined because of the issue of electronic self-interaction, but the exchange part in HF is precisely defined [15]. However, the results are unsatisfactory when the exchange part from HF and the correlation part from DFT are combined directly. This issue would be avoided by hybrid functionals, which incorporate DFT and HF and group the exchange and correlation components of each approaches. For instance, the B3LYP hybrid functional [16] is the most popular hybrid functional. It is spelt out as:

$$E_{XC}^{B3LYP} = E_X^{LDA} + a_0(E_X^{HF} - e_X^{LDA}) + a_X(E_X^{GGA} - E_X^{LDA}) + E_C^{LDA} + a_c(E_C^{GGA} - E_C^{LDA})$$ --(2.16)

Where E_X^{GGA} and E_C^{GGA} are the GGA exchange and correlation functionals, E_C^{LDA} is the LDA to the correlation functional, a_0 is set to 0.20, a_X is set to 0.72, a_C is set to 0.81.

In this thesis, we have primarily used the ωB97XD hybrid [17] to replicate the structural geometry of C_{18} nanocluster. It is a dispersion-corrected functional. For the simulation of Raman spectra, we have opted for the CAM-B3LYP hybrid functional [18].

2.3. Basis Sets

Atom-localized basis functions can be used to generate atomic or molecule orbitals. As a linear combination of these functions with certain coefficients, the orbitals are enlarged. They can be divided into two categories: Slater- and Gaussian-type orbitals (STOs and GTOs) [19].

$$\eta^{STO} = Nr^{n-1}e^{\zeta r}Y_l(\theta, \varphi)$$ ---- (2.17)

Where N is a normalization coefficient, ζ is the exponent, *r, θ, φ* are the spherical coordinaties, Y_{lm} represents the angular momentum component, n symbolises the principal quantum number, *l* defines the angular quantum number, and *m* represents the magnetic quantum number.

They can be expressed in the following way for the GTOs:

$$\eta^{GTO} = Nx^l y^m z^n e^{-r^2}$$ ---- (2.18)

N denotes the normalisation factor, while *x, y,* and *z* are Cartesian coordinates.

In general, the STOs have a spike at *r=0* and a nice exponential decay for greater values of *r*. These characteristics aid in accurately describing the hydrogen atomic orbitals. In contrast, GTOs do not have a peak at *r=0* and decay fast as *r* increases. The product of two GTOs, on the other hand, is a third one located between them, which is not the case for STOs. This trait eliminates the computationally expensive challenge of dealing with four-center-two-electron integrals. Combining numerous GTOs to simulate an STO is frequently more efficient than employing STOs directly.

The degree of complexity, or precision, of a basis set is defined as the number of contracted functions (CGF) necessary to represent each atomic orbital [20]. The STO-3G basis set, for example, is constructed by the linear combination of three CGF to represent a STO. Typically, double-zeta and triple-zeta basis sets provide adequate precision and system insight. The valence electrons are of great importance since they are the most involved in chemical

reactions. Hence, a flexible description of valence electrons is required. To achieve this goal, split valence basis sets are developed to treat the core and valence orbitals differently. The most widely used split valence basis set is the 6-31G basis set [21], which follows the nomenclature X-YZG. X is the number of primitive GTOs employed to describe one single contracted Gaussian function of the core. Y and Z are the number of primitive GTOs employed to describe the valence orbitals. By increasing the angular momentum, polarisation and diffuse functions can be introduced to the basis sets. For example, the 6-31G(d,p) basis set combines p and d polarisation functions. The diffuse functions are added to the 6-31+G basis set.

The GTO valence basis set is coupled with pseudopotentials in the SVP (split valence polarisation) type basis set [22]. The pseudopotentials will be discussed in the following section. This basis set includes a single basis function to describe the inner shell atomic orbitals, two basis functions to describe each valence shell atomic orbital, and a collection of polarisation functions. The 6-311G ++(d,p) level theory is mainly used in the present thesis. For the transition metal impurities, the former basis set is too small, that is why we have resorted to the LanL2DZ basis set [23].

2.4. Time Dependent Density Functional Theory (TD-DFT)

The DFT has been simplified to include time-dependent potentials and is now known as time-dependent density functional theory (TD-DFT). In the context of the time-dependent electron density $\eta(\boldsymbol{r},t)$, the TD-DFT is considered time-dependent quantum mechanics [24]. In 1984, Runge and Gross proposed the Runge-Gross theorem [25], which is related to the Hohenberg-Kohn theorem for time-dependent electron density. TD-DFT, unlike DFT, does not have a minimum energy concept. Rather, it is based on the notion of stationary action. It can offer an imaginary system of non-interacting electrons with the same density $\eta(\boldsymbol{r},t)$ as a real system that hops in time-dependent effective potential $v_{eff}(\boldsymbol{r},t)$ as DFT. This yields the time-dependent Kohn-Sham equation, which is identical to the time-dependent Schrödinger equation:

$$i\hbar\frac{\partial}{\partial t}\psi_i(\boldsymbol{r},t) = \left[\frac{-\hbar^2}{2m_e} + v_{eff}(\boldsymbol{r},t)\right]\psi_i(\boldsymbol{r},t) \text{ ---- (2.19)}$$

Here, $v_{eff}(\boldsymbol{r},t) = v_{ext}(\boldsymbol{r},t) + v_{XC}(\boldsymbol{r},t) + e^2\int k\frac{\eta(\boldsymbol{r}',t)}{|\boldsymbol{r}-\boldsymbol{r}'|}d^3\boldsymbol{r}'$, where $v_{XC}(\boldsymbol{r},t)$ indicates the time-dependent exchange-correlation potential and the unknown term has to be determined. The density therefore is given by:

$$\eta(\boldsymbol{r},t) = \sum_i |\psi_i(\boldsymbol{r},t)|^2 \text{---- (2.20)}$$

The adiabatic local density approximation [26] (ALDA), which uses uniform gas with the instantaneous density, is the simplest approximation for $v_{XC}(\boldsymbol{r},t)$.

$$v_{XC}^{ALDA}(\boldsymbol{r},t) = v_{XC}^{unif}[\eta(\boldsymbol{r},t)] \text{ ---- (2.21)}$$

Equation (2.29) calculates the excited state energies as well as the photo-absorption cross-section of molecules and clusters.

2.5. Properties from DFT for the Present Thesis

2.5.1. Vibrational Spectra Calculation

The optimization of molecular structural geometry aids in the prediction of IR and Raman spectra [27]. The frequency computation, which is independent of experimental investigation, provides the position and intensity of vibration of bands. The harmonic model is used to calculate the frequencies [28]. In practice, however, they are anharmonic. As a result, this describes the differences between experimental and calculated frequencies. The total energy of a molecule with N atoms adjacent to its equilibrium structure can be calculated as follows:

$$E = T_k + V_p = \frac{1}{2}\sum_{i=1}^{3N} q_i^2 + V_{eq} + \sum_{i=1}^{3N}\sum_{j=1}^{3N}\left(\frac{\partial^2 V}{\partial q_i \partial q_j}\right)_{eq} q_i q_j \text{ ---- (2.22)}$$

Where, q_i represents the mass-weighted Cartesian displacements and written as:

$$q_i = M_i^{\frac{1}{2}}(X_i - X_{ieq}) \text{ ---- (2.22)}$$

Where X_i is the position of the nuclei in relation to their equilibrium locations, M_i and X_{ieq} are the masses of the nuclei. The potential energy at the equilibrium nuclear conformation is denoted by V_{eq} in equation (2.30), and the extension of a power series is succinct at the second order. Therefore, the equation for classical mechanics can be expressed as:

$$Q_i = \sum_{i=1}^{3N} f_{ij} q_i \text{ ---- (2.23)}$$

Here, f_{ij} stands for the quadratic force constants calculated through: $f_{ij} = \left(\frac{\partial^2 V}{\partial q_i \partial q_j}\right)_{eq}$

It can be calculated through numerical second differentiation: $\frac{\partial^2 V}{\partial q_i \partial q_j} = \frac{\Delta(\Delta V)}{\Delta q_i \Delta q_j}$

The current thesis investigates Raman intensities as well as their vibrational modes in relation to potential energy distribution. The Raman intensities were computed in Gaussian 09 using the obtained Raman activities (S_i) and the intensity theory of Raman scattering [29] relationship:

$$I_i = \left[\frac{f(v_0 - v_i)^4 S_i}{v_i\{1-\exp(-\frac{hcv_i}{kT})\}}\right] \text{---- (2.24)}$$

In equation (2.33), v_0 represents the exciting wavenumbers in cm^{-1}, and v_i represents the vibrational wavenumber of the i^{th} normal mode. The universal constants *h, c,* and *k* are used, while *f* is a suitable common normalisation factor for all peak intensities.

2.5.2. Frontier Molecular Orbitals (FMO)

The development of a new set of orbitals comes from the overlap of two orbitals [30]. If the superimposition is overlooked, the difference in energy before and after the overlap is given by the second-order perturbation expression.

$$E = 2\sum_{l=1}^{n/2} \lambda_i \text{ ---- (2.25a)}$$

$$E = 2\sum_{l=1}^{(n-1)/2} \lambda_i + \lambda_{(n+1)/2} \text{ ---- (2.25b)}$$

If n is an even number, the (n/2) eigenvector indicates the highest (doubly) occupied molecular orbital (the HOMO), with an energy of $\lambda_n/2$. The following eigenvector is $(\lambda_n/2)+1$ for the lowest unoccupied molecular orbital (the LUMO), whose energy is. The HOMO-LUMO separation is then stated as:

$$\Delta HL = \frac{\lambda_n}{2} - \frac{\lambda_n}{2} + 1 \text{ ---- (2.26)}$$

2.5.3. Mulliken Charge Analysis

Mulliken charges, also referred to as partial charges [31], are a concept employed to elucidate the distribution of electronic charge within a molecule and to discern the characteristics of molecular orbitals concerning specific atom pairs, such as whether they exhibit bonding, anti-bonding, or nonbonding behaviour. To grasp the concept of these population matrices, let's take a brief look at a real and normalized molecular orbital composed of two similarly normalized atomic orbitals. The determination of Mulliken charges involves a straightforward multiplication process:

$$P_{ij} = D_{ij}S_{ij} \text{ ---- (2.27)}$$

In the above equation, the charge population matrix is denoted by P, the density matrix by D, and the overlap matrix by S.

2.5.4. Molecular Electrostatic Potential (MESP)

The molecular electrostatic potential is a very important parameter for explaining charge distribution and thus charge-related phenomena. It is useful in predicting the reactivity of hydrogen bonds and the relative polarity of molecules [32]. The charge distribution around the molecule in space helps visualise the reactive zone for electrophilic and nucleophilic attack. The MESP at a specific point in space around the molecule is expressed by:

$$V(\boldsymbol{r}) = \sum_A \frac{Z_A}{|\boldsymbol{R_A}-\boldsymbol{r}|} - \int \frac{\rho(\boldsymbol{r'})d\boldsymbol{r'}}{|\boldsymbol{r'}-\boldsymbol{r}|} \text{ ---- (2.28)}$$

Where, Z_A is the charge on the nucleus A, located at R_A, and ρ is the molecular electronic density function. The first term on the right hand side of the equation (2.35) indicates nuclei effects, whereas the second term represents electron effects. The mapping of an electron density iso-surface with a molecule's electrostatic potential surface illustrates the size, shape, charge density, and location of chemical reactivity (active site) of the molecules and offers the molecular electrostatic potential surface. The red colour symbolises low potential areas (excess of electrons), the blue colour represents high potential areas (void of electrons), and the green colour represents the neutral region (zero potential).

2.5.5. Topological Parameters and Quantum Theory of Atoms in Molecules

The Quantum Theory of Atoms in Molecules (QTAIM), which provides a thorough framework for comprehending the subtleties of hydrogen bonding inside molecules, is Bader's revolutionary contribution to the science of chemistry [33]. QTAIM relies on topological parameters, particularly the electron density (ρ_{BCP}) and the Laplacian of the electron density ($\nabla^2\rho_{BCP}$) at the Bond Critical Point (BCP), to provide crucial insights into the distribution of electron density and the distances between atoms. These parameters form the cornerstone of the theory of structural stability.

Hydrogen bonds, a vital aspect of molecular interactions, are contingent on specific conditions for their existence. The presence of a Bond Critical Point at the 'proton (H)-acceptor (A)' interface serves as confirmation of the occurrence of a hydrogen bonding interaction.

Consequently, hydrogen bond interactions in molecules can be categorized into three primary types:

(i) Strong Bonds (Covalent): These hydrogen bonds are characterized by a significant degree of electron sharing and represent robust interactions within the molecule.

(ii) Medium Bonds (Partially Covalent): Medium-strength hydrogen bonds exhibit a moderate level of electron sharing, striking a balance between covalent and non-covalent interactions.

(iii) Weak Bonds (Van der Waals): Weak hydrogen bonds primarily rely on van der Waals forces and exhibit minimal electron sharing, resulting in relatively weak intermolecular interactions.

2.5.6. Global Reactivity Parameters

In chemistry, reactivity is a significant concept that functions as a stimulus for chemical reactions and increases the physiochemical properties of molecules. Electrophilicity and nucleophilicity, which affect the reactivity and stability of molecules, are predicted using conceptual quantum mechanical descriptors or global reactivity parameters [34]. While Fukui functions and other local reactivity factors are employed to grasp active sites suitable for electrophilic and nucleophilic attacks in the molecular system [35].

The **chemical potential (μ)** of a molecule is defined as the amount of energy (U) received or released when the number of particles in a specific molecule varies at a constant external potential (V). It can also be expressed as the inverse of electronegativity χ. It is defined as follows:

$$\mu = \left(\frac{\partial U}{\partial N}\right)_V = -\chi \text{ ---- (2.29)}$$

Parr and Pearson postulated that chemical potential offers resistance to deform or modify the quantity of electrons during the charge transfer process. The **global hardness** can be defined as the second derivative of the energy (E) versus the number of electrons at a fixed external potential V(**r**):

$$\eta = \frac{1}{2}\left(\frac{\partial^2 E}{\partial N^2}\right)_{V(\boldsymbol{r})} \text{ ---- (2.30)}$$

The global softness (S) is inversely proportional the global hardness.

$$S = \frac{1}{2\eta} \text{ ---- (2.31)}$$

The **electrophilicity index (ω)** is a chemical reactivity metric used to understand global reactivity trends. A molecule with a lower ω value is a good nucleophile that is more reactive, whereas a molecule with a higher ω value is a good electrophile. When the system receives electrons from the environment, ω evaluates the donating tendency of the electrons.

$$\omega = \frac{\mu^2}{2\eta} \text{ ---- (2.32)}$$

2.5.7. Dipole Moments

The dipole moment (D) and polarizability (α) were calculated using the Gaussian 09 software and the finite field (FF) technique [36]. Buckingham's Cartesian coordinate definitions can offer them:

$$D = \left(D_x^2 + D_y^2 + D_z^2\right)^{\frac{1}{2}} \text{ ---- (2.33)}$$

$$< \alpha > = \frac{1}{3}\left(\alpha_{xx} + \alpha_{yy} + \alpha_{zz}\right) \text{ ---- (2.34)}$$

2.5.8. Ultraviolet (UV) Spectra

UV-Vis spectra offer valuable insights into the composition of samples, although their utility may be limited when it comes to distinguishing between different substances. Instead, UV-Vis spectroscopy is primarily employed for quantitative estimations. This technique relies on measuring the absorbance of light at specific wavelengths and applying the Beer-Lambert Law, which is a fundamental principle in spectrophotometry. The Beer-Lambert Law [37] states that when light passes through a sample or is reflected from it, the amount of light absorbed is determined by the difference between the incident light intensity (I_0) and the transmitted light intensity (I). This absorbed light is quantified as either absorbance or transmittance. The transmittance (T) is expressed as:

$$T = I/I_0 \text{ ---- (2.35a)}$$

$$\%T = \left(\frac{I}{I_0}\right)/100 \text{ ---- (2.34b)}$$

Whereas, the absorbance (A) is expressed by:

$$A = -\log T = \eta c r \text{ ---- (2.36)}$$

Where, η is the molar absorptivity, c stands for concentration, and r represents the sample size in cm. The absorbance relationship described above illustrates the direct

proportionality between absorbance and the number of molecules absorbing light. In the UV-Vis (ultraviolet-visible) region of the electromagnetic spectrum, incident photons carry energy that corresponds to electronic excitations from occupied orbitals to unoccupied orbitals within molecules. This energy difference between the ground state and the first excited state is precisely reflected in the longest wavelength absorbed by the molecule. For example, one common type of electronic transition in the UV-Vis region is the $\pi \rightarrow \pi^*$ transition. This transition occurs when the energy of the incident photons is equivalent to the energy difference between the bonding (π) and antibonding (π^*) orbitals of the molecule. In other words, when photons with the right energy are absorbed, they promote electrons from the π bonding orbital to the π^* antibonding orbital, leading to the observed absorption in the UV-Vis spectrum.

Understanding these electronic transitions and the associated energy differences is fundamental in interpreting UV-Vis spectra and gaining insights into the electronic structure and properties of molecules. It allows scientists to identify the types of bonds and electronic configurations present in a given molecule by analyzing the wavelengths of light it absorbs.

2.6. Gaussian 09 Package

Gaussian, a versatile computational chemistry software, traces its roots back to 1970 when it was introduced as Gaussian 70 by John Pople and his team at Carnegie Mellon University. The nomenclature "Gaussian" reflects Pople's innovative shift from Slater-type orbitals to Gaussian orbitals, a strategic move aimed at enhancing the efficiency of molecular electronic structure calculations. This adjustment proved pivotal, especially for computationally demanding methods like Hartree–Fock and hybrid Density Functional Theory (DFT), considering the limited computational capacities of the era.

Originally accessible through the Quantum Chemistry Program Exchange, Gaussian took a significant leap in 1987 when Gaussian, Inc. secured its licensing rights, marking a transformative moment in its commercial trajectory. Since then, Gaussian has undergone continuous updates and development, solidifying its status as a leading force in computational chemistry. The present thesis builds upon the capabilities of Gaussian 09, a notable version within the Gaussian software series, renowned for its prowess in computational chemistry. Through Gaussian 09, this work delves into molecular modelling, electronic structure calculations, and various facets of theoretical chemistry, benefiting from its reliability, versatility, and continuous advancements that have made it an indispensable tool for researchers in the field.

A sample input file for a hazardous gas NH_3 molecule is shown below:

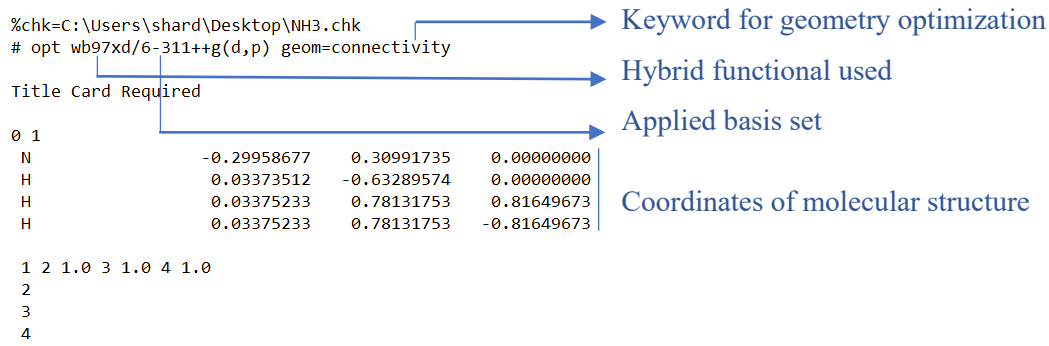

BIBLIOGRAPHY:

[1] M. J. Frisch, Trucks, G.W., Schlegel, H.B., Scuseria, G.E., Robb, M.A., Cheeseman, J.R., *Gaussian 09, Revis. A.02, Gaussian, Inc.*, 2016, 1–2.

[2] E. Schrödinger, *Phys. Rev.*, 1926, **28**, 1049–1070.

[3] M. Born and R. Oppenheimer, *Ann. Phys.*, 1927, **389**, 457–484.

[4] J. C. Slater, *Phys. Rev.*, 1929, **34**, 1293–1322.

[5] D. R. Hartree and W. Hartree, *Proc. R. Soc. London. Ser. A - Math. Phys. Sci.*, 1935, **150**, 9–33.

[6] J. C. Slater, 1951.

[7] P. Hohenberg, W. Kohn, Phys. Rev., 1964, **136**, B864.

[8] W. Kohn, L. J. Sham, Phys. Rev., 1964, **140**, A1133.

[9] W. Kohn, A. D. Becke and R. G. Parr, *J. Phys. Chem.*, 1996, **100**, 12974–12980.

[10] J. W. Negele, *Phys. Rev. C*, 1970, **1**, 1260–1321.

[11] J. P. Perdew and K. Burke, *Phys. Rev. B - Condens. Matter Mater. Phys.*, 1996, **54**, 16533–16539.

[12] P. M. W. Gill, B. G. Johnson, J. A. Pople and M. J. Frisch, *Chem. Phys. Lett.*, 1992, **197**, 499–505.

[13] K. Burke, J. P. Perdew and Y. Wang, *Electron. Density Funct. Theory*, 1998, 81–111.

[14] C. Adamo, M. Ernzerhof and G. E. Scuseria, *J. Chem. Phys.*, 2000, **112**, 2643–2649.

[15] A. D. Becke, *J. Chem. Phys.*, 1993, **98**, 1372–1377.

[16] K. Raghavachari, *Theor. Chem. Acc.*, 2000, **103**, 361–363.

[17] G. A. Dilabio, E. R. Johnson and A. Otero-De-La-Roza, *Phys. Chem. Chem. Phys.*, 2013, **15**, 12821–12828.

[18] T. Yanai, D. P. Tew and N. C. Handy, *Chem. Phys. Lett.*, 2004, **393**, 51–57.

[19] H. Stoll, G. Wagenblast and H. Preuß, *Theor. Chim. Acta*, 1980, **57**, 169–178.

[20] A. D. McLean and G. S. Chandler, *J. Chem. Phys.*, 1980, **72**, 5639–5648.

[21] V. A. Rassolov, J. A. Pople, M. A. Ratner and T. L. Windus, *J. Chem. Phys.*, 1998, **109**, 1223–1229.

[22] S. Genheden, A. Reymer, P. Saenz-Méndez and L. A. Eriksson, *Computational Chemistry and Molecular Modelling Basics*, 2017.

[23] S. Chiodo, N. Russo and E. Sicilia, *J. Chem. Phys.*, 2006, **125**, 1–8.

[24] K. Burke, J. Werschnik and E. K. U. Gross, *J. Chem. Phys.*, 2005, **123**, 1–34.

[25] E. Runge and E. K. U. Gross, *Phys. Rev. Lett.*, 1984, **52**, 997–1000.

[26] J. Harris, 1984.

[27] J. Neugebauer, M. Reiher, C. Kind and B. A. Hess, *J. Comput. Chem.*, 2002, **23**, 895–910.

[28] R. M. LEVY, *Ann. N. Y. Acad. Sci.*, 1986, **482**, 24–43.

[29] R. A. Cowley, *Proc. Phys. Soc.*, 1964, **84**, 281–296.

[30] A. Patel, 2020.

[31] R. S. Mulliken, *J. Chem. Phys.*, 1935, **3**, 586–591.

[32] J. S. Murray and P. Politzer, *Wiley Interdiscip. Rev. Comput. Mol. Sci.*, 2011, **1**, 153–163.

[33] R. F. W. Bader, *Acc. Chem. Res.*, 1985, **18**, 9–15.

[34] H. Chermette, *J. Comput. Chem.*, 1999, **20**, 129–154.

[35] P. Bultinck, R. Carbó-Dorca and W. Langenaeker, *J. Chem. Phys.*, 2003, **118**, 4349–4356.

[36] D. Tzeli and A. Mavridis, *J. Chem. Phys.*, 2005, **122**, 7–8.

[37] Beer, *Ann. der Phys. und Chemie*, 1852, **5**, 78–88.

[38] S. J. A. Pople, 2004.